Algorithmic decoherence time for decay-of-mixing non–Born–Oppenheimer dynamics

Shu Chun Cheng,[1] Chaoyuan Zhu,[1,a)] Kuo Kan Liang,[2] Sheng Hsien Lin,[1,2,3] and Donald G. Truhlar[4,b)]
[1]*Department of Applied Chemistry, Institute of Molecular Science and Center for Interdisciplinary Molecular Science, National Chiao-Tung University, Hsinchu 300, Taiwan*
[2]*Division of Mechanics, Research Center for Applied Sciences, Academia Sinica, Taipei 115, Taiwan*
[3]*Institute of Atomic and Molecular Sciences, Academia Sinica, Taipei 106, Taiwan*
[4]*Department of Chemistry and Supercomputing Institute, University of Minnesota, 207 Pleasant Street S.E., Minneapolis, Minnesota 55455-0431, USA*

(Received 29 February 2008; accepted 28 May 2008; published online 11 July 2008)

The performance of an analytical expression for algorithmic decoherence time is investigated for non–Born–Oppenheimer molecular dynamics. There are two terms in the function that represents the dependence of the decoherence time on the system parameters; one represents decoherence due to the quantum time-energy uncertainty principle and the other represents a back reaction from the decoherent force on the classical trajectory. We particularly examine the question of whether the first term should dominate. Five one-dimensional two-state model systems that represent limits of multidimensional nonadiabatic dynamics are designed for testing mixed quantum-classical methods and for comparing semiclassical calculations with exact quantum calculations. Simulations are carried out with the semiclassical Ehrenfest method (SE), Tully's fewest switch version (TFS) of the trajectory surface hopping method, and the decay-of-mixing method with natural switching, coherent switching (CSDM), and coherent switching with reinitiation (CSDM-D). The CSDM method is demonstrated to be the most accurate method, and it has several desirable features: (i) It behaves like the representation-independent SE method in the strong nonadiabatic coupling regions; (ii) it behaves physically like the TFS method in noninteractive region; and (iii) the trajectories are continuous with continuous momenta. The CSDM method is also demonstrated to balance coherence well with decoherence, and the results are nearly independent of whether one uses the adiabatic or diabatic representation. The present results provide new insight into the formulation of a physically correct decoherence time to be used with the CSDM method for non–Born–Oppenheimer molecular dynamic simulations. © *2008 American Institute of Physics*.
[DOI: 10.1063/1.2948395]

I. INTRODUCTION

The time-dependent Schrödinger equation governs the evolution of an entire isolated system, but unsolved questions arise when the entire system is divided into a quantum subsystem and its environment where the quantum subsystem is described by a Schrödinger equation, while its environment is described by classical mechanics. Upon such a division, the interaction of the subsystem with the environment induces decoherence that is formally defined by the loss of quantum coherence in the reduced density matrix obtained by tracing over the environment.[1–3] However, since the interaction between the system and its environment is not exactly known, the decoherence can only be evaluated with certain approximations in practical molecular dynamics simulations.

A general task facing all mixed quantum-classical approaches is how to treat the interaction between subsystems. If the goal is to simulate detailed quantum mechanical state-to-state transitions, this kind of division is not possible. Fortunately, most experimentally interesting observables involve only highly averaged quantities, and the goal of mixed quantum-classical approaches is to get those observables right by simulating the average quantum effects. Decoherence is one such quantum effect.

One example of a quantum-classical division is to treat electrons quantum mechanically and nuclei classically. When the quantal electrons do not evolve adiabatically, this leads to non–Born–Oppenheimer trajectories for nuclear motion. Two kinds of methods for treating these are the trajectory surface hopping (TSH) method[4–18] and the self-consistent semiclassical Ehrenfest (SE) method.[19–34] The TSH-type methods run trajectories on a single potential energy surface, usually an electronically adiabatic one, until the trajectory switches instantaneously to another surface, and the SE-type methods run trajectories on an average (mean-field) potential energy surface. Both types of method are widely applied for nonadiabatic molecular dynamic simulations.[35]

The trajectory-surface-hopping-based approaches[4–18] switch trajectories from one electronic potential energy surface to another by adjusting a component of the momentum along the hopping direction to maintain energy conservation.

a)Electronic mail: cyzhu@mail.nctu.edu.tw.
b)Electronic mail: truhlar@t1.chem.umn.edu.

When this hop is not possible due to an insufficient energy component along the hopping direction, the attempted hop is called a frustrated hop. The fewest switches with time-uncertainty (FSTU) method,[15] FSTU grad V method,[13] and FSTU with stochastic decoherence (FSTU/SD) method[18] can improve the Tully's fewest switch (TFS) method[6] by making some, but not all, of the frustrated hops allowed. Because surface hopping methods do not describe decoherence correctly, they are very sensitive to the representation (adiabatic or diabatic) in which trajectories are simulated.

The conventional self-consistent SE approach[19–28] is expected to be most accurate for coherent events, but the coherent mean-field trajectory is not able to describe the case in which a trajectory is required to decohere to a single electronic state asymptotically. Nevertheless, the SE method provides a good framework for further work when considered together with the quantum-classical Liouville equation (the reader is referred to recent theoretical work on quantum-classical and semiclassical Liouville equations for nonadiabatic transitions for appropriate background[29,36–46] and discussion of the proper treatment of coherence and decoherence). It is by following this approach, we hope, that the goal of rigorously deriving efficient algorithms for the trajectory-based treatment of classical-quantum dynamics on coupled electronic surfaces may be realized. Using this approach, we showed that the main feature that needs to be incorporated from the Liouville equation is decoherence.[29] In order to include this decoherence into the mean-field approaches, Hack and Truhlar[30] proposed the natural decay-of-mixing (NDM) method so that the mean-field state is replaced by a decohering state by adding decay into the coupled electronic Schrödinger equations. The decohering state behaves like the mean-field state when the system is in a strong interaction region, but the decohering state gradually decoheres into a mixture of pure electronic states when a system leaves the interaction region. Because the decoherence is built into the quantal evolution of the electronic motion, it naturally induces an extra force acting back on the classical nuclear motion. This force is called the decoherence force or decoherent force, and it is determined in part by the requirement of energy conservation. The decoherence force drives each trajectory from the decay-of-mixing electronic potential energy surface to a pure electronic potential energy surface. This decay-of-mixing trajectory leads to more accurate non–Born–Oppenheimer transition probabilities than either the mean-field or surface hopping trajectory.[30]

The decohering states are dynamically mixed electronic states that decohere to a particular pure electronic state when all coupling terms vanish for a certain period of time. Instead of describing a nonadiabatic transition as sudden hopping from one pure-state electronic potential energy surface to another, as in TSH methods, decay-of-mixing methods[29,30,32–34] describe the switching gradually. The TFS switching algorithm is employed in the natural decay-of-mixing method, i.e., the TFS switching probability is utilized to control switching from one decoherent state to another.

The NDM switching probability balances coherence with decoherence inappropriately. To improve this situation, we devised the self-consistent decay-of-mixing method[32] in which we replace the derivative of the decohering electronic wave function by its coherent component while calculating the switching probability. This does improve the decay-of-mixing method. We then further improved the decay-of-mixing method by assuming that the switching probability is governed by only the coherent parts of the coupled electronic Schrödinger equations.[29,33,34] This is called coherent switching (CS) with decay of mixing (CSDM), and it is the best decay-of-mixing method we have established so far.

In the decay-of-mixing methods, even in the gas phase, the nuclear degrees of freedom are considered as a kind of bath. Electronically nonadiabatic transitions are formulated within the density matrix framework by including decay of off-diagonal elements of the density matrix, with the decay governed by a decoherence time. Even though we have no precise method for establishing the decoherence time, we have shown that this approach is successful for three-dimensional (3D) nonadiabatic molecular collisions.[29,33–35]

One-dimensional model problems can be useful for illustrating how coherence effects are averaged out in real molecular collisions. It is possible because of the simplicity of the one-dimensional world and the paucity of outgoing channels in one-dimensional systems, that one-dimensional problems can be less sensitive to approximations than 3D problems. In practice though, problems involving just one degree of freedom are often more sensitive to the parameter choices than are 3D cases.[4] The goal of the present paper is to see if the examination of one-dimensional systems can provide a way to improve the expression for decoherence time.

In the Sec. II, we briefly review the decay-of-mixing method with three switching algorithms. Section III analyzes the algorithmic decoherence time, and Sec. IV presents five one-dimensional models for representative types of nonadiabatic systems. Section V presents concluding remarks.

II. DECAY-OF-MIXING METHODS

We review the theory in terms of the density matrix formalism by starting with electronic motion. The equation of motion for an element of the density matrix is[29]

$$\dot{\rho}_{kk'} = \dot{\rho}^{C}_{kk'} + \dot{\rho}^{D}_{kk'}, \tag{1}$$

where C and D denote coherent and decoherent contributions to the rate of change. The coherent term is given in a general representation (that is, adiabatic, diabatic, or part way in between) by

$$i\hbar\dot{\rho}^{C}_{kk'} = \sum_{l} (\rho_{lk'}[U_{kl} - i\hbar\dot{\mathbf{R}}\cdot\mathbf{d}_{kl}] - \rho_{kl}[U_{lk'} - i\hbar\dot{\mathbf{R}}\cdot\mathbf{d}_{lk'}]), \tag{2}$$

where k and k' label electronic states ($k,k'=1,2,\ldots,m$, where m is the number of electronic states), $\mathbf{R}$ is an N-dimensional vector of nuclear coordinates, an overdot denotes a time derivative, and $U_{kk'}$ is symmetric potential energy matrix which is defined as containing the matrix elements of the electronic Hamiltonian H_{el},

$$U_{kk'} = \langle k|H_{\rm el}|k'\rangle. \tag{3}$$

The nonadiabatic coupling vector $\mathbf{d}_{kk'}$ is an $m\times m$ anti-Hermitian matrix in electronic state space, and each element is a vector in $\mathbf{R}$,

$$\mathbf{d}_{kk'} = \langle k|\nabla_{\mathbf{R}}|k'\rangle, \tag{4}$$

where $\nabla_{\mathbf{R}}$ is the N-dimensional nuclear gradient. In the adiabatic representation, $\mathbf{U}$ is a diagonal matrix called $\mathbf{V}$; and one can define a "diabatic" representation where $\mathbf{d}_{kk'}$ is approximated as zero and $\mathbf{U}$ is not diagonal. The decoherent part of the rate of change of the density matrix $\dot{\rho}^D_{kk'}$ is discussed below.

The Hamiltonian governing the nuclear motion trajectory can be written as

$$H = \frac{\mathbf{P}^2}{2\mu} + \sum_k \rho_{kk}U_{kk} + \sum_k \sum_{k'<k} 2\,\mathrm{Re}(\rho_{kk'})U_{kk'}. \tag{5}$$

We solve the equations in an isoinertial, mass-scaled nuclear-coordinate system $\mathbf{R}$ in which coordinates associated with all nuclear masses are scaled to the same reduced mass μ. The momentum conjugate to $\mathbf{R}$ is called $\mathbf{P}$. The nuclear motion is represented by a swarm of classical trajectories, and the nuclear position and momentum of each trajectory evolve according to classical equations of motion,

$$\dot{\mathbf{R}} = \nabla_{\mathbf{P}}H = \mathbf{P}/\mu, \tag{6}$$

$$\dot{\mathbf{P}} = -\nabla_{\mathbf{R}}H = \dot{\mathbf{P}}^C + \dot{\mathbf{P}}^D, \tag{7}$$

where the coherent part is given as[29]

$$\dot{\mathbf{P}}^C(t) = -\sum_k \rho_{kk}\nabla_{\mathbf{R}}U_{kk} - \sum_k \sum_{k'<k} (2\,\mathrm{Re}\,\rho_{kk'})\nabla_{\mathbf{R}}U_{kk'} + \sum_j \sum_k \sum_{k'} (2\,\mathrm{Re}\,\rho_{kj})U_{kk'}\mathbf{d}_{k'j}. \tag{8}$$

The second term in Eq. (7) is the decoherent force and is given by

$$\dot{\mathbf{P}}^D = -\frac{\mu\dot{V}^D}{\mathbf{P}\cdot\hat{\mathbf{s}}}\hat{\mathbf{s}}, \tag{9}$$

with

$$\dot{V}^D = \sum_k \dot{\rho}^D_{kk}U_{kk} + \sum_k \sum_{k'<k} 2\,\mathrm{Re}(\dot{\rho}^D_{kk'})U_{kk'}. \tag{10}$$

The unit vector $\hat{\mathbf{s}}$ represents the direction into which energy is deposited and out of which energy is consumed. The diagonal parts of the decoherent contribution to the rate of change of the density are

$$\dot{\rho}^D_{ii} = \begin{cases} -\dfrac{\rho_{ii}}{\tau_{iK}}, & i\neq K \\ \displaystyle\sum_{j\neq K}\frac{\rho_{jj}}{\tau_{Kj}}, & i=K \end{cases}, \tag{11}$$

where K denotes the decoherent state, and off-diagonal terms modeled[29] only as nonlinear in this article (as we focus on decoherence time),

$$\dot{\rho}^D_{ij} = \begin{cases} -\dfrac{1}{2}\left(\dfrac{1}{\tau_{iK}}+\dfrac{1}{\tau_{jK}}\right)\rho_{ij}, & i\neq K,\quad j\neq K \\ \dfrac{1}{2}\left(\dfrac{1}{\rho_{KK}}\displaystyle\sum_{k\neq K}\frac{\rho_{kk}}{\tau_{Kk}}-\frac{1}{\tau_{jK}}\right)\rho_{ij}, & i=K,\quad j\neq K \\ \dfrac{1}{2}\left(\dfrac{1}{\rho_{KK}}\displaystyle\sum_{k\neq K}\frac{\rho_{kk}}{\tau_{Kk}}-\frac{1}{\tau_{iK}}\right)\rho_{ij}, & i\neq K,\quad j=K \end{cases}, \tag{12}$$

in which τ_{ij} is the decoherence time, which is also called the decay time. Three switching methods are considered in the present study in both adiabatic and diabatic representations.

II.A. Natural switching (NS)

NS is a direct application of Tully's fewest switching probability: for example, in the two-state case, the probability of switching from decoherent state K to some other state K' between time t and time $t+dt$ is given by

$$P_{K\to K'} = \max\left(-\frac{\dot{\rho}_{KK}dt}{\rho_{KK}},0\right) = \max\left(-\frac{(\dot{\rho}^C_{KK}+\dot{\rho}^D_{KK})dt}{\rho_{KK}},0\right). \tag{13}$$

In this case, the density matrix elements that define the decay-of-mixing method are fully used to calculate the switching probability. This can be also called uncoherent switching.

II.B. CS

The CS algorithms differs from Eq. (13) in that the density matrix that governs trajectories is no longer used to calculate the switching probability. We define a new set of coherent state populations $\tilde{\rho}_{KK'}$ which are obtained from Eq. (1) without $\tilde{\dot{\rho}}^D_{KK'}$. Then,

$$P_{K\to K'} = \max\left(-\frac{\tilde{\dot{\rho}}_{KK}dt}{\tilde{\rho}_{KK}},0\right). \tag{14}$$

This is called global CS; $\tilde{\rho}_{KK'}$ is the same as in the fully coherent SE method except that the trajectory is not the SE trajectory. We could call $\rho_{KK'}$ the trajectory density matrix and $\tilde{\rho}_{KK'}$ the CSDM density matrix.

II.C. CS with reinitialization (CS-D)

Global CS in Sec. II B involves two density matrices; these are also used in the CS-D algorithm. In CSDM-D, though, in order to eliminate coherent interference between two consecutive nonadiabatic coupling regions, we reinitialize the CSDM density matrix to the trajectory density matrix at minima of $D_K(t)$, which is defined as

$$D_K(t) = \sum_j |d_{Kj}|^2. \tag{15}$$

This reinitialization creates the switching method called CSDM-D.

III. DECOHERENCE TIME

For all proposed decay-of-mixing methods and switching algorithms, the decay time and the decoherent direction must be specified to completely specify the computational simulation method. In the one-dimensional case, the decoherence direction is already specified since there is only one possible direction in nuclear-coordinate space. The absence of coupling between the choice of decoherence direction and the choices of expression and parameters for the decoherecne time is one of the reasons why one-dimensional models might help to illuminate the most physical choice of the decoherence time.

In a previous study[47] we have derived an expression for the decoherence time based on the principles enunciated by Paz *et al.*,[48] namely, (i) that the semiclassical limit of a wave function is the sum of Wentzel-Kramers-Brillouin-like trajectories associated with minimum wave packets, and decoherence of the superposition is faster than decoherence of the individual packets (nuclear wave packets move at different speeds on different surfaces and get out of phase and out of overlap) and (ii) that the pointer basis is the one in which decoherence is the fastest. Using these principles led to a decoherence time given by

$$\frac{1}{\tau_{kk'}} = \frac{1}{\tau^{\Delta F}} + \sqrt{\left(\frac{1}{\tau^{\Delta p}}\right)^2 + \left(\frac{1}{\tau^{\Delta F}}\right)^2}, \tag{16}$$

where $\tau^{\Delta F}$ is a complicated expression that accounts for the different forces on the two surfaces, and

$$\tau^{\Delta p} = \frac{\hbar}{|U_{kk} - U_{k'k'}|}\sqrt{\frac{4\pi^2|p_k - p_{k'}|}{\bar{p}}}, \tag{17}$$

which accounts for the decoherence due to wave packets moving with different speeds on different surfaces. In Eq. (17), p_k is the momentum on surface k, $p_{k'}$ is the momentum on surface k', and $\bar{p}$ is their average. For parallel surfaces in one dimension, Eq. (16) reduces to $\tau = \tau^{\Delta p}$. Unfortunately, although we can use Eq. (16) in conjunction with surface hopping,[18] we cannot use it with the decay-of-mixing algorithms because they require

$$\frac{1}{\tau_{kK}} \xrightarrow{\mathbf{P}\cdot\hat{\mathbf{s}}\to 0} (\mathbf{P}\cdot\hat{\mathbf{s}})^n, \quad n > 1, \tag{18}$$

in order that demixing does not occur when the momentum in the decoherent direction is insufficient to provide the required energy.[33] Therefore we must substitute an algorithmic decoherence time for the physical one. The required algorithmic decoherence time is whatever makes the ensemble average over the CSDM trajectories agree best with accurate quantum results for the rate of change of populations and coherences and, ultimately, for the final state populations.[49]

The decay time function we used in the previous study was[34]

$$\tau_{kK} = \frac{\hbar}{|V_{kk} - V_{KK}|}\left(1 + \frac{E_0}{(\mathbf{P}\cdot\hat{\mathbf{s}})^2/2\mu}\right), \tag{19}$$

where E_0 is a parameter that was taken as 1 a.u. The first term in Eq. (16) is a truly quantal contribution from the quantum mechanical time-energy uncertainty relation, but the second term in Eq. (19) represents a back reaction from the classical trajectory due to the decoherence force. Although Eq. (19) performs acceptably well, it is not ideal. In particular, for algorithmic decoherence time, it can confuse the physical meaning of the decoherence time when the second term in Eq. (19) contributes more than the first term; in addition, the second term can cause rapid oscillatory structure in density matrix elements. Therefore, we reconsider an earlier form that we have used,[33] in particular,

$$\tau_{Kk} = \frac{c_1\hbar}{|V_{KK} - V_{kk}|} + \frac{C_2\hbar}{(\mathbf{P}\cdot\hat{\mathbf{s}})^2/2\mu}, \tag{20}$$

where two coefficients in Eq. (20) are adjustable. Note that we sometimes use the notation, $c_1 = C_1\pi$. Equation (20) was obtained in Ref. 33 by a series of approximations based on the shortest self-consistent decay time, with explanation that the first term should contribute more to decoherence time.

The high-energy limit is an important limiting case. Equations (16)–(20) all have the physically correct feature that decoherence slows down when the momentum component in the nonadiabatic coupling direction is small. Furthermore, if the collision energy is much higher than the potential gap $|V_{KK} - V_{kk}|$, the contribution from the second term usually becomes negligible, and in this case, the decoherence time is entirely from the first term of Eq. (20).

For a two-state system, the prefactor in Eqs. (17) and (19) is the shortest time scale in the system. Therefore one knows from general principles[50] that c_1 must be greater than or equal to unity. Our previous experience with 3D collisions as well as exploratory work on one-dimensional collisions had indicated that values somewhat larger than unity work best, perhaps even values as large as ~6. Yet we recognize the importance of making the decay as fast as possible so that decoherence decays between strong interaction regions, an algorithmic decision that builds on the work of Gislason and co-workers[7,13,51] and whose necessity was spelled out particularly clearly in work by Thachuk *et al.*[24] Therefore in the present work we explore c_1 values larger than unity, up to ~9, in particular, $c_1 = 0.5\pi$, π, 2π, and 3π, that is, $C_1 = 0.5$, 1, 2, and 3.

IV. FIVE ONE-DIMENSIONAL TEST MODELS

To begin this section, we make a few remarks about one-dimensional cases, in general. In one dimension, there is no initial vibrational phase, rotational orientation, impact parameter, or impact angle to average over. In fact, the SE results are based on a single trajectory in each case, and the other methods require averaging only because of the stochastic nature of the surface hops and the switches in decoherent state. Furthermore, even including these stochastic events, one-dimensional trajectories exhibit much less diversity than multidimensional trajectories. For example, in one dimension, the direction of motion of the trajectory is always parallel or antiparallel to the nonadiabatic coupling vector, and when all states are energetically accessible all trajectories pass through the same points in space. The smaller amounts of averaging and path diversity have the consequence that

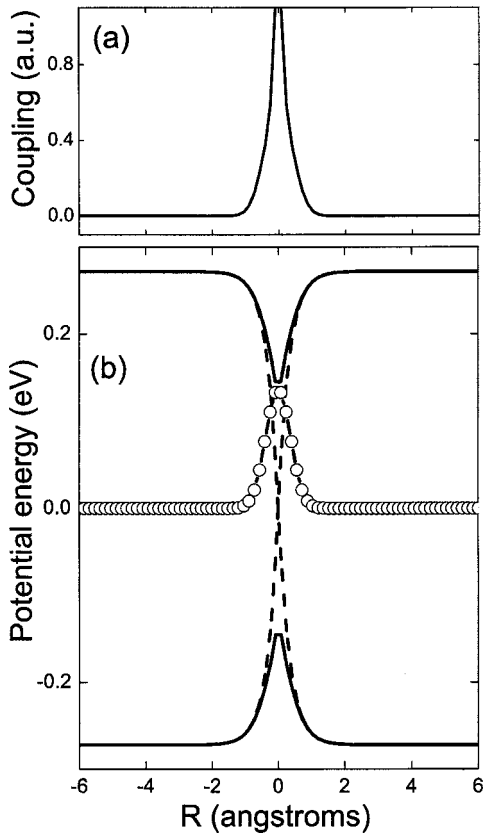

FIG. 1. Potential energy curves V_i and U_{ij} and nonadiabatic coupling $\mathbf{d}_{12}$ for model I, the simple avoided crossing case. (a) The solid line represents the nonadiabatic coupling $\mathbf{d}_{12}$. (b) The solid lines represent adiabatic potential curves V_i, the dashed lines represent diabatic potential curves U_{ii}, and the open circles represent the diabatic coupling curves U_{12}.

oscillatory structure in the energy dependence of the transition probabilities is much more likely to be observed in semiclassical calculations in one-dimensional problems than in multidimensional ones, even if two strong-coupling regions are moved far apart. It is known from previous work on vibrational-rotational energy transfer collisions[52–56] and chemical reactions[57,58] that reduced-dimensional models often do not work well. In addition it is known that one-dimensional electronically nonadiabatic collisions are much more sensitive than full-dimensional collisions to the details of the coupling.[4,59] Furthermore the character of surface crossings and avoided crossings is far more complex in multidimensional problems than in one dimension.[60] However, we focus on the decoherence time in the present study, and if a given prescription for the decoherence time works well in one-dimensional dynamics; we believe that it deserves further study in multidimensional cases as well.

In the rest of this article, the decay-of-mixing methods with NS (NDM), CS (CSDM), and CS with reinitiation (CSDM-D) plus the FSTU surface hopping method and the SE mean-field method are applied to five one-dimensional model systems in both the adiabatic and the diabatic representations. We focus on how the three decay-of-mixing switching methods vary with change of decoherence time.

Figures 1–4 correspond to model I, which has a simple avoided crossing with only one strong-coupling region. Figures 5 and 6 correspond to model II, which has two

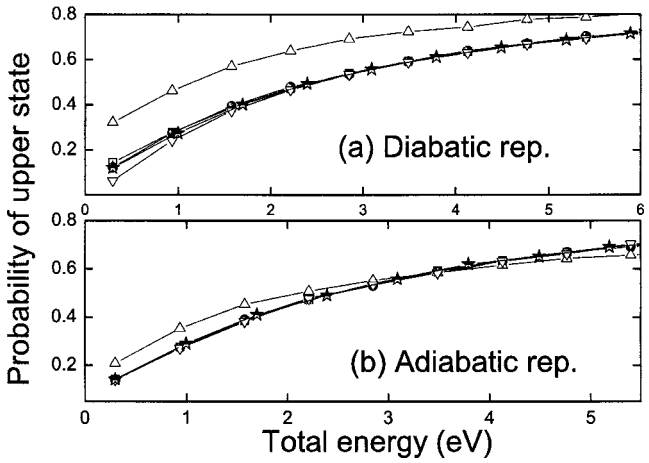

FIG. 2. Nonadiabatic transition probabilities for model I. All semiclassical results are calculated in both the (a) diabatic (d) and (b) adiabatic (a) representations. The exact quantum mechanical results are not plotted as they are almost identical to those from the SE method. The open squares represent the SE method. The solid balls represent the CSDM method. The upper half full stars represent the CSDM-D method. The open up triangles represent the NDM method. The open down triangles represent FSTU method.

avoided crossings and two strong-coupling regions. Models I and II represent Landau–Zener–Teller–type[61–64] interactions that are similar to those found in the 3D MXH system (see Ref. 65, for instance).

Figures 7–11 correspond to model III, with two regions in each of which the adiabatic potential curves cross twice, but with the diabats approximately parallel rather than crossing. This gives four strong-coupling regions; model III represents Rosen–Zener–Demkov–type[66,67] interactions that are similar to those found in the 3D YRH system (see Ref. 68, for instance).

Figures 12–14 correspond to model IV, which is designed to show the effect of a potentially strongly dephasing region between two avoided crossings. Figures 15 and 16 correspond to model V, which has ten avoided crossings and represents an attempt to design a one-dimensional system with the multiple strong-coupling encounter characteristic of a multidimensional trajectory.

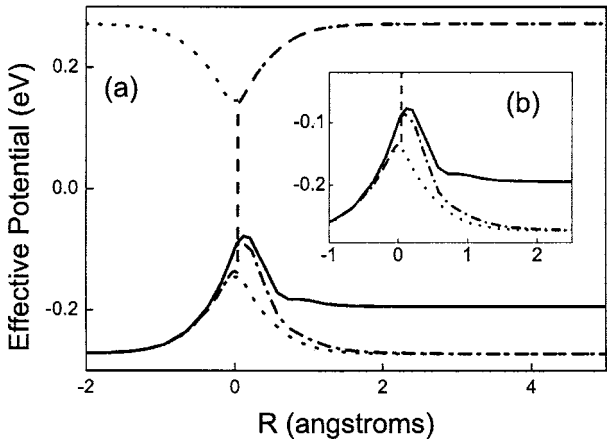

FIG. 3. (a) Effective potentials (including decay of mixing) are calculated along a trajectory with different methods for model I in Fig. 1. The dots represent original adiabatic potential curves in Fig. 1. The solid lines represent the SE method. The dashed lines represent the FSTU method. The dashed-dot lines represent the CSDM and CSDM-D methods with no switching. Part (b) is zooming the strong-coupling region of (a).

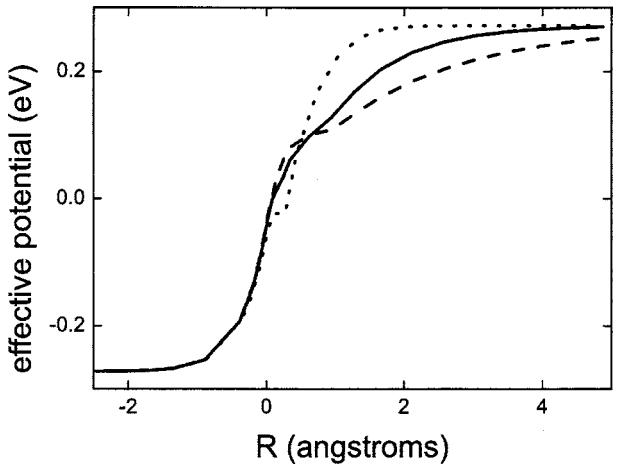

FIG. 4. Effective potentials for CSDM and CSDM-D methods with switching turned on are plotted for different C_1 and C_2 in model I. The dot lines represent C_1, $C_2=3,0.5$. The solid lines represent C_1, $C_2=1,0.5$ and the dashed lines represent C_1, $C_2=0.5,0.5$.

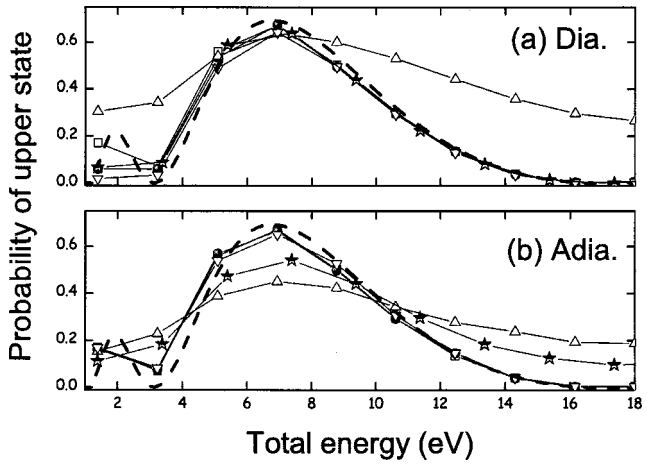

FIG. 6. Nonadiabatic transition probabilities for model II. All symbols and notation are the same as in Fig. 2 except that the exact results are plotted as dashed lines.

The overall probability of a nonadiabatic transition reported here is defined as the probability of starting on the lower potential surface at $R=-\infty$ and finishing on the upper potential surface at $R=+\infty$. Accurate numerical quantum mechanical calculations for the five one-dimensional two-state cases were performed using the conventional time-independent close-coupling method[69] with a reduced mass $\mu=1.097216$ amu for all five-model systems. The accurate quantum mechanical results are independent of representation, and the calculations are carried out in the diabatic representation. Semiclassical simulations are carried out by using the Bulirsch–Stoer[70] and modified midpoint method[71] for integrating the trajectories. The number of trajectories for each energy is 10 000 for all five models in both the adiabatic and diabatic representations, except for the SE method, where only one trajectory is necessary. In practice, a starting point of $R=-5$ Å and an ending point of $R=+5$ Å are satisfactory for models I–III, and termini of $R=\pm 7$ Å are satisfactory for models IV and V. Note that the SE method gives the same results in the adiabatic and diabatic representations, and this is verified numerically in every case.

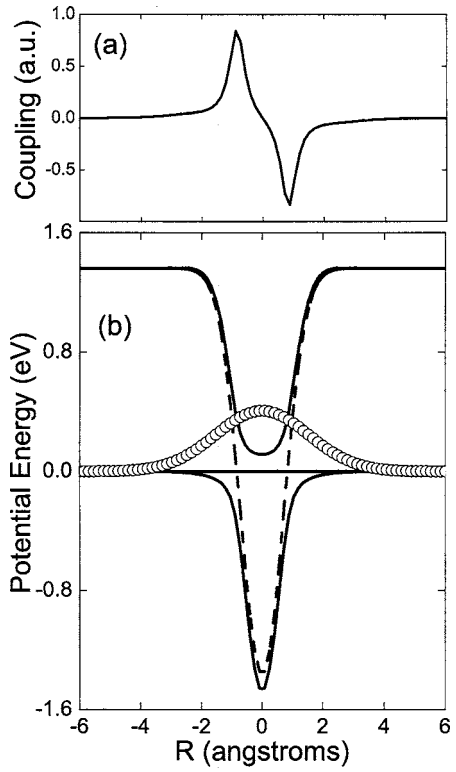

FIG. 5. Potential energy curves and nonadiabatic coupling for model II, the dual avoided crossing case. The symbols are the same as in Fig. 1.

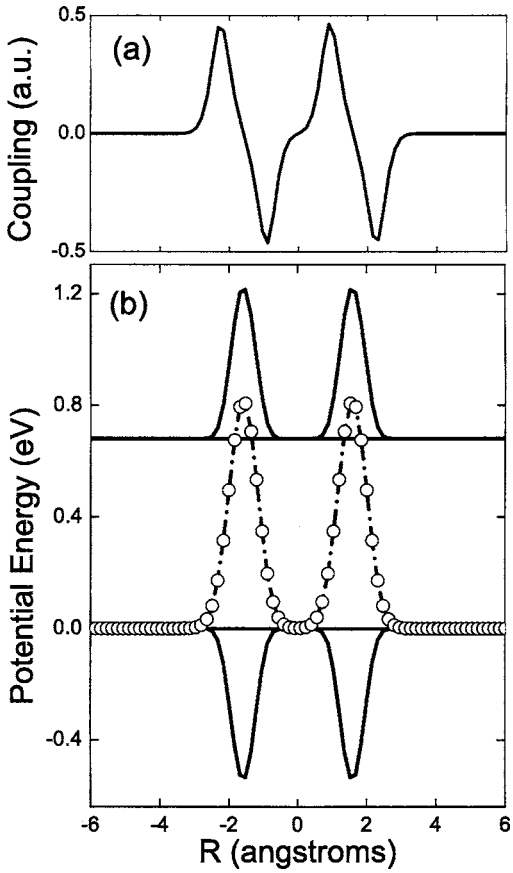

FIG. 7. Potential energy curves and nonadiabatic coupling for model III, the Rosen–Zener–Demkov case. The symbols are the same as in Fig. 1.

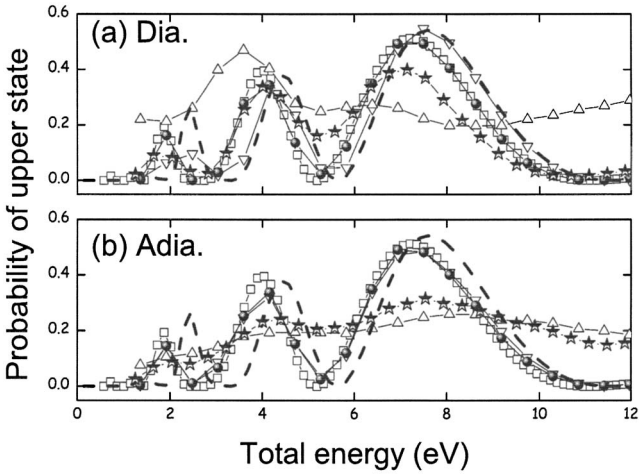

FIG. 8. Nonadiabatic transition probabilities for model III. All symbols and notation are the same as in Fig. 2 except that the exact results are plotted as dashed lines.

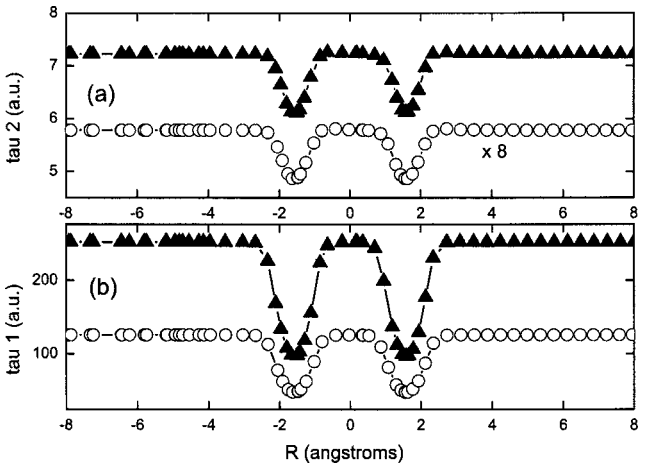

FIG. 10. Comparisons of the two terms in the decoherence time in Eq. (20) for model III with different C_1 and C_2. (a) is for the second term in Eq. (20); the filled triangles linked by dash-dot lines represent $C_2=0.75$ ($C_1=2$), and the open circles linked by dashed lines represent $C_2=0.075$ ($C_1=1$). Part (b) is for the first term; all symbols are the same as in plot (a).

All five one-dimensional model problems are studied at energies where both potential energy curves are energetically accessible at all values of the coordinate R. Thus, there are no frustrated hops in the one-dimensional studies presented here.

Before considering the results, it is useful to discuss the goal. As stated in the Introduction, our goal is for the semiclassical results to agree with the fully quantum mechanical ones, at least on the average. In addition, where possible, it is preferable to reproduce the oscillations due to coherence. One can retain the most coherence by using the Ehrenfest method, but the SE method is not accurate enough for many purposes, and experience in a variety of contexts has shown that better results may be obtained with methods that do not include full coherence.[7,18,23,24,27–34,49,51,65,72–75] In developing design objectives, we should keep in mind that oscillations in transition probabilities as a function of a collision parameter such as the incident energy are sometimes a quantum effect on nuclear motion, not a direct observation of electronic state amplitudes. For example, oscillations sometimes occur in single-electronic-state problems where electronic decoherence is not a problem. A complete analysis of where the oscillations come from in each case would be difficult and might not be informative because we know from previous experience that the same oscillation can show up in one way in one semiclassical method and in another way in another.[76] One way to reproduce the oscillations in general molecular collisions would have to include all interference between trajectories, as in classical S matrix theory.[77] A considerable effort was invested in this kind of work in the 1970s, and various lessons emerged, including these. (1) Although it is possible to include interference effects in simple systems such as nonreactive, single-surface collinear collisions of at-

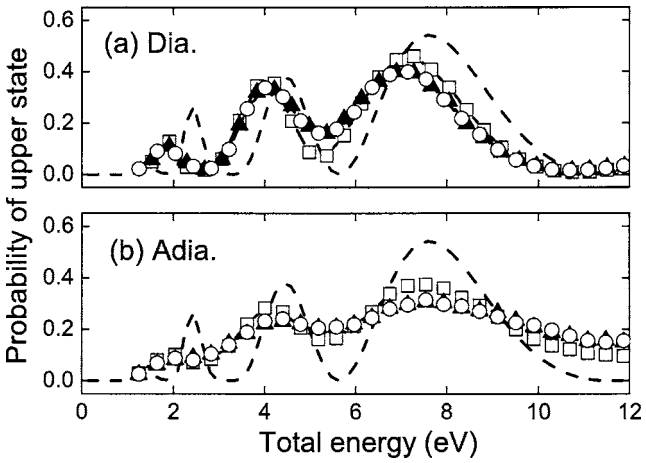

FIG. 9. Nonadiabatic transition probabilities calculated by CSDM-D method with different C_1 and C_2 for model III. (a) in diabatic representation and (b) in adiabatic representation. The dash lines are exact results. The open circles stand for $C_1=1$ and $C_2=0.75$. The closed up triangles stand for $C_1=1$ and $C_2=0.075$ and the open square stand for $C_1=2$ and $C_2=0.075$.

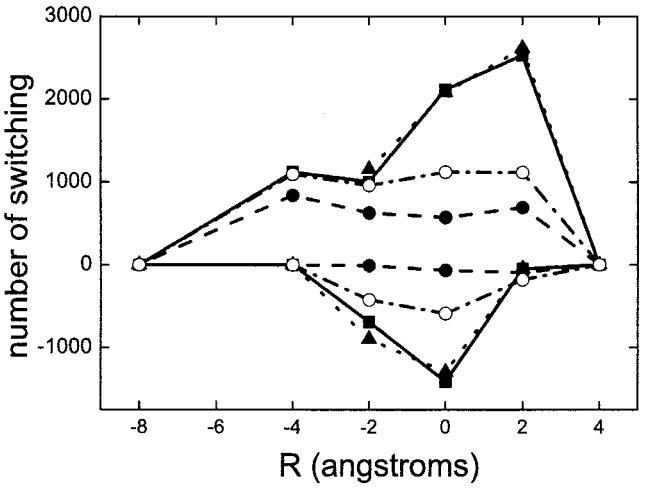

FIG. 11. Number of decoherent-state switch events in the ensemble in simulations with 10 000 trajectories for model III. Simulations are carried out in the adiabatic representation at total energy of 7.6 eV for various methods; the closed squares linked by solid lines are for the FSTU method, the filled triangles linked by dot lines are for CSDM method, the open circles linked by dashed-dot lines are CSDM-D, and the closed circles linked by dash lines are NDM. Positive values stand for the number of switches from the lower to the upper decoherent state, and the negative values stand for those from the upper to the lower decoherent state.

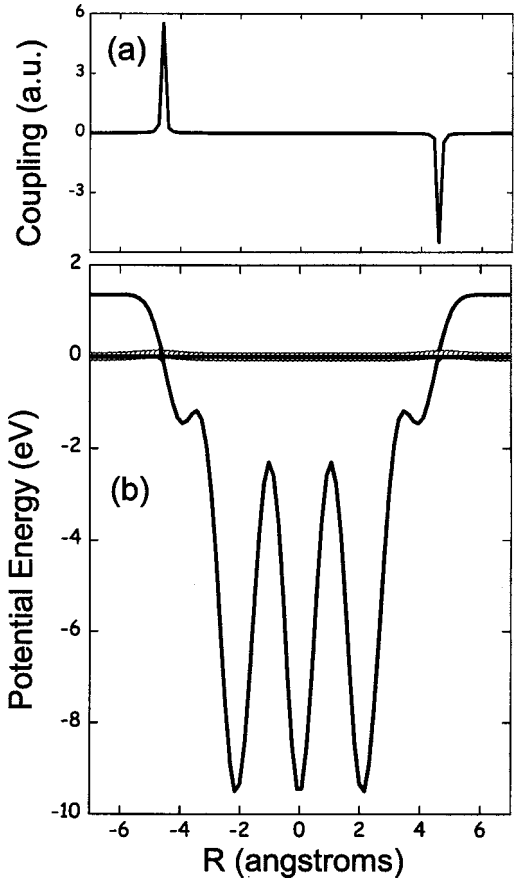

FIG. 12. Potential energy curves and nonadiabatic coupling for model IV. The symbols are the same as in Fig. 1.

oms with diatoms, it becomes very hard to do so for realistic systems such as chemical reactions in full dimensionality. (2) It is not necessary to include such oscillations in most applications because they usually average out when one sums over impact parameters (orbital angular-momentum quantum numbers) and averages over initial angular-momentum projection states (m states). Thus, as we stated in the second paragraph of the paper, the goal of our work is to obtain

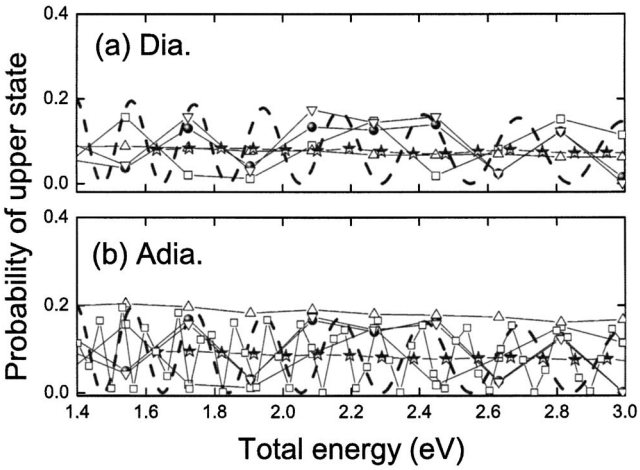

FIG. 13. Nonadiabatic transition probabilities for model IV. All symbols and notation are the same as in Fig. 2 except that the exact results are plotted as dashed lines.

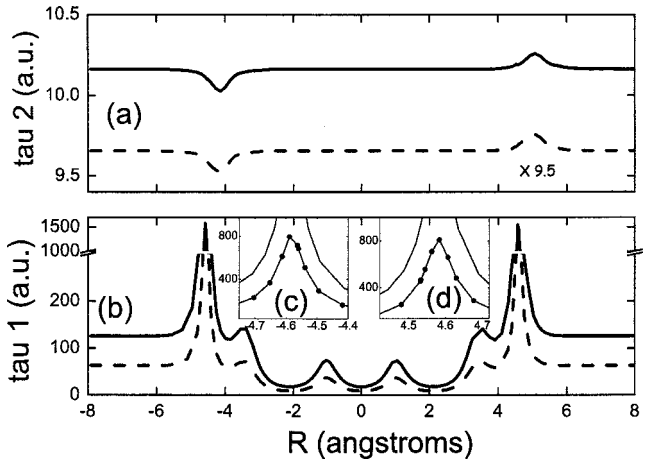

FIG. 14. Comparisons of the two terms in the decoherence time of Eq. (20) for model IV with different C_1 and C_2. Part (a) is for the second term in Eq. (20); the dashed lines represent $C_2=0.075$ ($C_1=1$) and the solid lines represent $C_2=0.75$ ($C_1=2$). Part (b) is for the first term; all symbols are the same as in plot (a). Parts (c) and (d) are zooming in the two strong-coupling regions with $R\approx\pm4.6$ Å in (b).

semiclassical transition probabilities that agree with accurate results on the average. We have shown previously that the CSDM method does this more accurately than other methods that have been proposed, such as surface hopping or the SE method. The present test cases will provide an opportunity to test this even in cases where the oscillations are not averaged

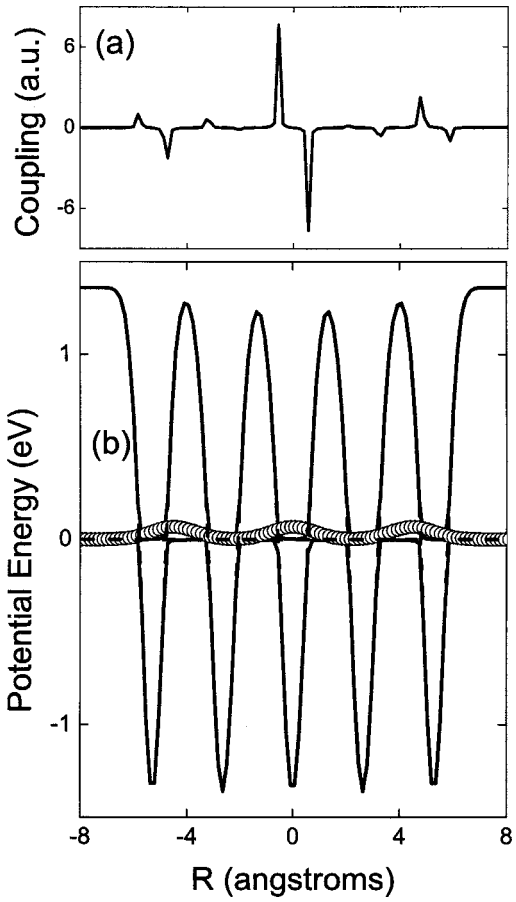

FIG. 15. Potential energy curves and nonadiabatic coupling for model V. The symbols are the same as in Fig. 1.

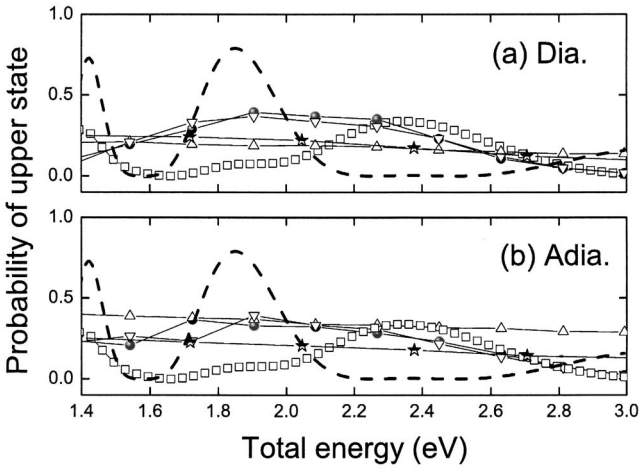

FIG. 16. Nonadiabatic transition probabilities for model V. All symbols and notation are the same as in Fig. 2 except that the exact results are plotted as dashed lines. For this figure $C_1=1$ and $C_2=0.5$.

out. Further discussion of the differences between one-dimensional model systems and real systems is provided elsewhere.[78]

IV.A. Simple avoided crossing (model I)

The model problems are all defined in the diabatic representation. Model I is defined by[8]

$$\begin{aligned} U_{11}(R) &= A[1-\exp(-BR)], \quad R>0, \\ U_{11}(R) &= -A[1-\exp(BR)], \quad R<0, \\ U_{22}(R) &= -U_{11}(R), \\ U_{12}(R) &= U_{21}(R) = C\exp(-DR^2), \end{aligned} \tag{21}$$

with $A=0.2721$ eV, $B=3.024$ Å^{-1}, $C=0.1351$ eV, and $D=3.571$ Å^{-2}. Figure 1(a) shows the nonadiabatic coupling, and Fig. 1(b) shows the potential curve and diabatic coupling. The energy gap between potential curves is 0.5442 eV in either asymptotic region. This model represents the simplest kind of nonadiabatic problem; it has only a single strong-coupling region.

The caption to Fig. 2 mentions that the SE calculations are almost identical with the quantum mechanical results [so we do not show exact results in Figs. 2(a) and 2(b)]. The transition probabilities calculated from FSTU, CSDM, and CSDM-D agree very well in both the adiabatic representation in Fig. 2(a) and the diabatic representation in Fig. 2(b). The NDM results show a slight deviation from the exact results and a strong representation dependence as well. All decay-of-mixing methods in Fig. 2 are calculated with $C_1=1$ and $C_2=0.5$. By consideration of all the results in Fig. 2, we conclude that if there is only one strong interaction region along a trajectory (this situation would be uncommon in real multidimensional systems), the switching probability should be computed from a completely coherent passage. Figures 3 and 4 show effective potential; these are computed from the trajectory density matrix. By calculating effective potential along one specific trajectory, Fig. 3 shows that effective potential in a strong-coupling zone is almost same for the SE and CSDM methods, but once leaving an interaction zone the CSDM effective potential approaches the original lower adiabatic potential, while the SE effective potential still stays on an average of the original two adiabatic potentials. Furthermore, Fig. 4 shows three CSDM effective-potential curves for $C_1=3$, 1, and 0.5, respectively, with fixed $C_2=0.5$, in which we can see that $C_1=1$ shows reasonable switching smoothness. Thus this example contributes to finding the best compromise motivated at the end of Sec. III; in particular, $C_1=1$ (that is, $c_1\approx 3$) provides a good compromise of retaining the fastest time scale in the system as the decoherence time (which would involve $C_1=1/\pi$), and making C_1 very large, which would ensure the smoothest possible effective potential.

IV.B. Dual avoided crossings (model II)

The model potential for system II is given in the diabatic representation by[8]

$$\begin{aligned} U_{11}(R) &= 0, \\ U_{22}(R) &= -A\exp(-BR^2)+E_0, \\ U_{12}(R) &= U_{21}(R) = C\exp(-DR^2), \end{aligned} \tag{22}$$

with the parameters chosen to be $A=2.721$ eV, $B=1.004$ Å^{-2}, $E_0=1.361$ eV, $C=0.4082$ eV, and $D=0.2143$ Å^{-2}. This model has two peaks in the nonadiabatic coupling, as shown in Fig. 5(a), so there are two distinct strong-coupling regions with a distance of 1.6616 Å between the peaks. Note that the diabatic coupling in Fig. 5(b) shows only one peak, but $\mathbf{d}_{12}$ (not U_{12}) is the correct measure of coupling strength in both representations.

The results of the SE, FSTU, and CSDM calculations follow the exact quantum oscillatory nonadiabatic transition probabilities fairly well except at low energies in both the adiabatic and the diabatic representation in Figs. 6(a) and 6(b). The NDM method shows strong representation dependence, and the CSDM-D method shows weak dependence due to reinitiation at the middle point. We conclude that the global CSDM method does contain a good balance between coherence and decoherence for reproducing quantum oscillatory features of the nonadiabatic transition probabilities in the one-dimensional case. All decay-of-mixing methods in Fig. 6 are calculated with $C_1=1$ and $C_2=0.5$ in Eq. (20). This model problem is more direct than our previous 3D tests in showing the ability of the CSDM algorithm to treat coherence while still maintaining c_1 small enough (~ 3) to achieve the fastest allowed decay between regions of strong interaction, as discussed in Sec. III.

IV.C. Dual Rosen–Zener–Demkov case (model III)

We define model III as two parallel diabatic potentials with diabatic coupling expressed in terms of two Gaussian functions,

$$U_{11}(R) = 0,$$

$$U_{22}(R) = A, \tag{23}$$

$$U_{12}(R) = U_{21}(R) = C[\exp(-D(R - R_0/2)^2) + \exp(-D(R + R_0/2)^2)],$$

with the parameters chosen to be $A=0.6803$ eV, $C=0.8163$ eV, $R_0=3.175$ Å, and $D=2.857$ Å^{-2}. Each diabatic coupling peak shown in Fig. 6(b) corresponds to two nonadiabatic coupling peaks; therefore this model has four peaks of the nonadiabatic coupling in Fig. 7(a), and there are four distinct strong-coupling regions.

The SE and CSDM calculations in both representations of Figs. 8 reproduce the oscillatory structure of the quantum results, although they are slightly out of phase for all energies. We have carried out more systematic tests in which we varied the distance R_0 between the interaction regions, and (although we do not show results here) the SE and CSDM results eventually become out of phase compared to more rapid oscillatory structure of the accurate quantal nonadiabatic transition probability as the distance between distinct interaction regions increases; nevertheless, the amplitude of the transition probability from the SE and CSDM methods is still within the envelope produced by the rapid quantum oscillations. We conclude again that the CSDM method does contain good balance between coherence and decoherence for reproducing quantum oscillatory features of nonadiabatic transition probabilities in the one-dimensional case.

The diabatic FSTU results agree with the quantum results better than the SE results, but FSTU calculations using the adiabatic representation in Fig. 8(b) are almost the same as the SE results. Both NDM and CSDM-D results show strong representation dependence again with the CSDM-D method in the diabatic representation containing more oscillatory structure as shown in model II. All decay-of-mixing methods in Fig. 8 are calculated with $C_1=1$ and $C_2=0.5$.

We investigate the CSDM-D method further in Fig. 9 by selecting three different sets of C_1 and C_2. We find nonadiabatic transition probabilities calculated by CSDM-D do not show strong dependence on C_1 and C_2, and the probabilities show about the same amount of oscillatory structure in the diabatic representation, as was shown in Fig. 8.

Figure 10 shows the change of decoherence time in Eq. (20) along two trajectories; Fig. 10(b) shows the first term in Eq. (20) and Fig. 10(a) shows the second term. It is easily understand that the first term doubles when C_1 is increased from 1 to 2 in Fig. 10(b). However, the second term does not increase by a factor of 10 when C_2 is increased from 0.075 to 0.75 in Fig. 10(a); this is because different trajectories are associated with the different C_1 so the momentum in the second term of Eq. (20) is not the same in the two cases. Furthermore, with the present choice of $C_1=1$ and $C_2=0.5$, we do see that the first term contributes more to the decoherence time than does the second term. This makes the model more physical.

Figure 11 shows number of trajectories switching from decoherent state 1 to decoherent state 2, and from 2 to 1 in 10 000 trajectories in the simulation. First of all, we can see that the number of switches from state 1 to state 2 is much greater than the number from state 2 to state 1 for all FSTU, CSDM, CSDM-D, and NDM methods. Second, we see that the number of switches is almost the same for the FSTH and CSDM methods. The numbers of switches in the CSDM-D and NDM methods are much less than in CSDM, especially that for the NDM method, for which there is no back switch from state 2 to state 1.

This model problem shows that the CSDM method, with the compromise value of $C_1=1$ selected in Sec. IIB, treats the coherence with equal accuracy to the SE method, which is fully coherent. Furthermore, this model shows that results of useful accuracy are satisfactorily obtained in a parameter range where the physical first term of Eq. (20) dominates the decoherence time expression as compared to the algorithmically required the second term. Finally, examination of the number of switches in various algorithms shows that the adoption of the fewest-switch criterion[8] for switching the decoherent state is a critical component of its success and explains why the CSDM method balances coherence with decoherence so well.

IV.D. Dynamically separated dual avoided crossings (model IV)

The fourth model has two widely separated distinct interaction regions between which the adiabatic or diabatic motions on the upper and lower surfaces are enormously different. The problem is designed to show how those motions influence the nonadiabatic transition probability, especially the oscillations. Figure 12(a) shows two sharp nonadiabatic coupling peaks, and Fig. 12(b) shows the potential curves. Model IV is given in the diabatic representation as

$$U_{11}(R) = 0,$$

$$U_{22}(R) = -AW_f + E_0, \tag{24}$$

$$U_{12}(R) = U_{21}(R) = V_0[\exp(-D(R - R_0)^2) + \exp(-D(R + R_0)^2)],$$

where

$$W_f = \exp(-B_1(R - R_1)^2) + \exp(-B_2(R - R_2)^2) + \exp(-B_0R^2) + \exp(-B_1(R + R_1)^2) + \exp(-B_2(R + R_2)^2), \tag{25}$$

with $A=2.721$ eV, $E_0=1.361$ eV, $V_0=0.0544$ eV, $D=1.071$ Å^{-2}, $B_0=B_1=1.786$ Å^{-2}, $B_2=1.428$ Å^{-2}, $R_0=4.763$ Å, $R_1=3.970$ Å, and $R_2=2.117$ Å.

We see in Fig. 13 that there are very rapid oscillations in the exact quantum mechanical nonadiabatic transition probability. The SE results in Figs. 13(b) get out of phase and oscillate even more rapidly than the quantum mechanical results. The FSTU and CSDM results in Figs. 13(a) and 13(b) are out of phase too and oscillate less rapidly than the exact calculations. The envelope of the transition probability calculated by the FSTU and CSDM methods in both representations follows the envelope of the exact calculation well. The NDM and CSDM-D methods show no oscillations in the nonadiabatic transition probability; the CSDM-D method does well on average as shown in Fig. 13 in both represen-

tations, while the NDM method shows strong representation dependence and overestimates the exact results on average in the adiabatic representation shown in Fig. 13(b). All decay-of-mixing methods in Fig. 13 are calculated with $C_1=1$ and $C_2=0.5$. The CSDM method performs equally well in both representations again.

Figure 14 shows change of decoherence time in Eq. (20) along two trajectories; Fig. 14(b) shows the first term in Eq. (20) and Fig. 14(a) shows the second term. The first term again doubles when C_1 is increased from 1 to 2 in Fig. 14(b), but the second term does not increase by a factor of 10 when C_2 is increased from 0.075 to 0.75 in Fig. 14(a) for the same reason as explained previously. We confirm again that with the present choice of $C_1=1$ and $C_2=0.5$, the decoherence time from the first term contributes much more than that from the second term.

This model problem has shown that the CSDM method with the compromise value of $C_1=1$ selected in Sec. IIB provides good average accuracy even when the fully coherent SE method does not reproduce the coherent oscillations. Furthermore, we report the encouraging finding that with parameters that yield good transition probabilities on the average, the physical first term of Eq. (20) again (as for the previous model problem) dominates the algorithmically required second term so that the results are not sensitive to the coefficient of the second term; this is important because the second term is the term where the algorithmic decoherence time must differ from the physical one for the reason explained in Sec. III, and achieving this relative magnitude of the two contributions to the decoherence time was the key motivation for adopting the new expression, as discussed in Sec. III.

IV.E. Multiple avoided crossings (model V) and summary

The fifth model is a multiple crossing case with ten distinct interaction regions for nonadiabatic couplings, as shown in Fig. 15(a). At least in this aspect it may be the most realistic test case since real multidimensional problems often have many distinct interaction regions. Figure 15(b) shows that the diabatic coupling has three local maxima. Model V is given in the diabatic representation by

$$U_{11}(R)=0,$$

$$U_{22}(R)=-AW_f+E_0, \tag{26}$$

$$U_{12}(R)=U_{21}(R)=V_0[\exp(-D(R-R_0)^2)+\exp(-DR^2)+\exp(-D(R+R_0)^2)],$$

where

$$W_f=\exp(-B_1(R-R_1)^2)+\exp(-B_2(R-R_2)^2)+\exp(-B_0R^2)+\exp(-B_1(R+R_1)^2)+\exp(-B_2(R+R_2)^2), \tag{27}$$

with careful choice of all parameters; $A=2.721$ eV, $E_0=1.361$ eV, $V_0=0.0680$ eV, $D=0.714$ Å^{-2}, $B_0=B_2=2.143$ Å^{-2}, $B_1=2.678$ Å^{-2}, $R_0=4.498$ Å, $R_1=5.292$ Å, and $R_2=2.646$ Å.

The SE results in Fig. 16(b) show oscillatory structure but are out of phase in comparison with quantum mechanical calculations and are not good on average. The FSTU, CSDM-D, and CSDM results in Figs. 15(a) and 15(b) are in reasonable agreement with the exact quantum mechanical results on average in both the adiabatic and diabatic representations. The NDM method does well on average in the adiabatic representation as shown in Fig. 15(b), but the NDM shows strong representation dependence again.

This model problem shows that the parameters selected in previous subsections, including a value of $C_1=1$ that represents a good compromise of two competing demands as discussed above and a value of $C_2=0.5$ that makes the algorithmic term less important than the time-uncertainty term, give good results on the average for a problem for which Ehrenfest does not give a good result on average. In summary, we find that CSDM with and $C_2=0.5$ gives reasonably good results, at least on the average, in every case.

V. CONCLUDING REMARKS

The decoherence time in Eq. (20) has been extensively investigated for five one-dimensional two-state models for five kinds of non–Born–Oppenheimer molecular dynamics methods, namely, the SE, FSTU, NDM, CSDM, and CSDM-D methods. The five one-dimensional models are representatives of various typical multidimensional nonadiabatic transition situations where the potential energy surfaces show characteristic features. Transition probabilities are compared to exact quantum mechanical results to learn how well decoherence effects are treated.

The CSDM method is confirmed to be the best method for balancing coherence with decoherence for nonadiabatic molecular dynamics simulations. With regard to switching, the CSDM method shows similar behavior to the surface hopping method, in part because of adapting the fewest-switch algorithm to a new context. This can be seen in Fig. 11 for model III. The CSDM method is shown to be insensitive to whether the simulation is performed in the adiabatic or diabatic representation; this is inherited from the SE method that is independent of representation. In strong nonadiabatic coupling regions, the CSDM trajectories are similar to the SE trajectories as can be seen in Fig. 3 for model I. Both the CSDM and CSDM-D methods are insensitive to the coefficients appearing in the decoherence time, and so there is no loss of accuracy if we require the first term of the decoherence time in Eq. (20) to dominate. Although an exact expression for the decoherence time is not known, it is reasonable to use a model in which the time-energy uncertainty relation is the major determining source of decohernece time. Therefore, Eq. (20) is quite reasonable for calculating the algorithmic decoherence time to be used with the CSDM method for non–Born–Oppenheimer molecular dynamics simulations.

ACKNOWLEDGMENTS

This work is supported by National Science Council of the Republic of China under Grant No. 96-2113-M-009-021 and by the National Science Foundation under Grant No. CHE07-04974. C.Z. would like to thank the MOE-ATU project of the National Chiao Tung University for the support.

[1] D. Giulini, E. Joos, C. Kiefer, J. Kupsch, I. Stamatescu, and H. D. Zeh, *Decoherence and the Appearance of a Classical World in Quantum Theory* (Springer-Verlag, Berlin, 1996).
[2] H. Breuer and F. Petruccione, *The Theory of Open Quantum Systems* (Oxford University Press, New York, 2002).
[3] W. Zhu and H. Rabitz, J. Chem. Phys. **118**, 6751 (2003).
[4] J. C. Tully and R. K. Preston, J. Chem. Phys. **55**, 562 (1971).
[5] P. J. Kuntz, J. Kendrick, and W. N. Whitton, Chem. Phys. **38**, 147 (1979); A. Bjerre and E. E. Nikitin, Chem. Phys. Lett. **1**, 179 (1967); E. E. Nikitin, M. Y. Ovchninikova, and D. V. Shalashilin, Chem. Phys. Lett. **111**, 313 (1987).
[6] N. C. Blais and D. G. Truhlar, J. Chem. Phys. **79**, 1334 (1983).
[7] G. Parlant and E. A. Gislason, J. Chem. Phys. **91**, 4416 (1989).
[8] J. C. Tully, J. Chem. Phys. **93**, 1061 (1990).
[9] G. Parlant and M. H. Alexander, J. Chem. Phys. **92**, 2287 (1990).
[10] D. F. Coker and L. Xiao, J. Chem. Phys. **102**, 496 (1995).
[11] M. Sizun, J.-B. Song, and E. A. Gislason, J. Chem. Phys. **109**, 4815 (1998).
[12] M. D. Hack, A. W. Jasper, Y. L. Volobuev, D. W. Schwenke, and D. G. Truhlar, J. Phys. Chem. A **103**, 6309 (1999).
[13] D. Babikov, E. A. Gislason, M. Sizun, F. Aguillon, and V. Sidis, J. Chem. Phys. **112**, 7032 (2000).
[14] M. D. Hack, A. W. Jasper, Y. L. Volobuev, D. W. Schwenke, and D. G. Truhlar, J. Phys. Chem. A **104**, 217 (2000).
[15] A. W. Jasper, S. N. Stechmann, and D. G. Truhlar, J. Chem. Phys. **116**, 5424 (2002); **117**, 10247(E) (2002).
[16] C. Zhu, H. Kamisaka, and H. Nakamura, J. Chem. Phys. **116**, 3234 (2002).
[17] A. W. Jasper and D. G. Truhlar, Chem. Phys. Lett. **369**, 60 (2003).
[18] A. W. Jasper and D. G. Truhlar, J. Chem. Phys. **127**, 194306 (2007).
[19] H.-D. Meyer and W. H. Miller, J. Chem. Phys. **70**, 3214 (1979).
[20] H.-D. Meyer and W. H. Miller, J. Chem. Phys. **72**, 2272 (1980).
[21] D. A. Micha, J. Chem. Phys. **78**, 7138 (1983).
[22] M. Amarouche, F. X. Gadea, and J. Durup, Chem. Phys. **130**, 145 (1989).
[23] A. Garcia-Vela, R. B. Gerber, and D. G. Imre, J. Chem. Phys. **97**, 7242 (1992).
[24] M. Thachuk, M. Y. Ivanov, and D. M. Wardlaw, J. Chem. Phys. **109**, 5747 (1998).
[25] D. A. Micha, Adv. Quantum Chem. **35**, 317 (1999).
[26] J. Mavri, Mol. Simul. **23**, 389 (2000).
[27] M. D. Hack and D. G. Truhlar, J. Phys. Chem. A **104**, 7917 (2000).
[28] M. D. Hack, A. W. Jasper, Y. L. Volobuev, D. W. Schwenke, and D. G. Truhlar, J. Phys. Chem. A **104**, 217 (2000).
[29] C. Zhu, A. W. Jasper, and D. G. Truhlar, J. Chem. Theory Comput. **1**, 527 (2005).
[30] M. D. Hack and D. G. Truhlar, J. Chem. Phys. **114**, 9305 (2001).
[31] K. F. Wong and P. J. Rossky, J. Chem. Phys. **116**, 8429 (2002).
[32] C. Zhu, A. W. Jasper, and D. G. Truhlar, J. Chem. Phys. **120**, 5543 (2004).
[33] C. Zhu, S. Nangia, A. W. Jasper, and D. G. Truhlar, J. Chem. Phys. **121**, 7658 (2004).
[34] A. W. Jasper, S. Nangia, C. Zhu, and D. G. Truhlar, Acc. Chem. Res. **39**, 101 (2006).
[35] See the Proceedings of the Faraday Discussion "Non-Adiabatic Effects in Chemical Dynamics," University of Oxford, UK, 5–7 April 2004, Royal Society of Chemistry (Cambridge, UK, 2004), Vol. 127, p. 1.
[36] A. Donoso and C. C. Martens, J. Phys. Chem. **102**, 4291 (1998).
[37] R. Kapral, J. Chem. Phys. **110**, 8919 (1999).
[38] S. Nielsen, R. Kapral, and G. Ciccotti, J. Chem. Phys. **112**, 6543 (2000).
[39] A. Donoso and C. C. Martens, J. Chem. Phys. **112**, 3980 (2000).
[40] C.-C. Wan and J. Schofield, J. Chem. Phys. **112**, 4447 (2000).
[41] C.-C. Wan and J. Schofield, J. Chem. Phys. **116**, 494 (2002).
[42] D. MacKernan, R. Kapral, and G. Ciccotti, J. Phys.: Condens. Matter **14**, 9069 (2002).
[43] I. Horenko, C. Salzmann, B. Schmidt, and C. Schütte, J. Chem. Phys. **117**, 11075 (2002).
[44] A. Sergi, D. Mac Kernan, G. Ciccotti, and R. Kapral, Theor. Chem. Acc. **110**, 49 (2003).
[45] I. Burghardt, K. B. Møller, G. Parlant, L. S. Cederbaum and E. R. Bittner, Int. J. Quantum Chem. **100**, 1153 (2004).
[46] I. Horenko, M. Weiser, B. Schmidt, and C. Schütte, J. Chem. Phys. **120**, 8913 (2004).
[47] A. W. Jasper and D. G. Truhlar, J. Chem. Phys. **123**, 64103 (2005).
[48] J. P. Paz, S. Habib, and W. H. Zurek, Phys. Rev. D **47**, 488 (1993).
[49] D. G. Truhlar, in *Quantum Dynamics of Complex Molecular Systems*, Springer Series in Chemical Physics Vol. 83, edited by D. A. Micha and I. Burghardt (Springer, Berlin, 2007), pp. 227–243.
[50] W. H. Zurek, Rev. Mod. Phys. **75**, 715 (2003).
[51] M. Sizun, J. B. Song, and E. A. Gislason, J. Chem. Phys. **109**, 4815 (1998).
[52] J. D. Kelley and M. Wolfsberg, J. Chem. Phys. **53**, 2967 (1970).
[53] M. H. Alexander, J. Chem. Phys. **61**, 5167 (1974).
[54] H. J. Korsch and V. Philipp, Chem. Phys. Lett. **31**, 296 (1975).
[55] W. R. Gentry and C. F. Giese, in *Atom-Molecule Collision Theory*, edited by R. B. Bernstein (Plenum, New York, 1979), pp. 391–425.
[56] N. Snider, J. Chem. Phys. **73**, 5659 (1980).
[57] J. N. L. Connor, W. Jakubetz, J. Manz, and J. C. Whitehead, Chem. Phys. **39**, 395 (1979).
[58] J. B. Song and E. A. Gislason, Chem. Phys. **202**, 1 (1996).
[59] S. L. Mielke, G. J. Tawa, D. G. Truhlar, and D. W. Schwenke, Chem. Phys. Lett. **234**, 57 (1995).
[60] T. C. Allison, G. C. Lynch, D. G. Truhlar, and M. S. Gordon, J. Phys. Chem. **100**, 13575 (1996); D. G. Truhlar and C. A. Mead, Phys. Rev. A **68**, 032501 (2003).
[61] L. D. Landau, Phys. Z. Sowjetunion **2**, 46 (1932).
[62] C. Zener, Proc. R. Soc. London, Ser. A **137**, 696 (1932).
[63] E. C. G. Stückelberg, Helv. Phys. Acta **5**, 369 (1932).
[64] E. Teller, J. Chem. Phys. **41**, 109 (1937).
[65] Y. L. Volobuev, M. D. Hack, M. S. Topaler, and D. G. Truhlar, J. Chem. Phys. **112**, 9716 (2000).
[66] N. Rosen and C. Zener, Phys. Rev. **40**, 502 (1932).
[67] Yu. N. Demkov, J. Exp. Theor. Phys. **45**, 195 (1963); Yu. N. Demkov, [Sov. Phys. JETP **18**, 138 (1966)]; Yu. N. Demkov, Dokl. Akad. Nauk SSSR **166**, 1076 (1966); Yu. N. Demkov, [Sov. Phys. Dokl. **11**, 138 (1966)].
[68] A. W. Jasper, M. D. Hack, and D. G. Truhlar, J. Chem. Phys. **115**, 1804 (2001).
[69] J. C. Light and R. B. Walker, J. Chem. Phys. **65**, 4272 (1976).
[70] R. Bulirsch and J. Stoer, Numer. Math. **8**, 1 (1966).
[71] W. H. Press, S. A. Teukolsky, W. T. Vetterling, and B. P. Flannery, *Numerical Recipes*, 3rd ed. (Cambridge University Press, Cambridge, 2007).
[72] E. R. Bittner and P. J. Rossky, J. Chem. Phys. **103**, 8130 (1995).
[73] B. J. Schwartz, E. R. Bittner, O. V. Prezhdo, and P. J. Rossky, J. Chem. Phys. **104**, 5942 (1996).
[74] O. V. Prezhdo and P. J. Rossky, J. Chem. Phys. **107**, 825 (1997).
[75] E. R. Bittner and P. J. Rossky, J. Chem. Phys. **107**, 8611 (1997).
[76] D. G. Truhlar and J. W. Duff, Chem. Phys. Lett. **36**, 551 (1975).
[77] W. H. Miller, J. Chem. Phys. **53**, 3578 (1970).
[78] D. Kohen, F. H. Stillinger, and J. C. Tully, J. Chem. Phys. **109**, 4713 (1998).